Analysis of the Atmospheric Effects on the Vicarious Calibration of LAPAN-A3/IPB Satellite Multispectral Camera in Jaddih Hill Madura

Sartika Salaswati[1], Patria Rachman Hakim[2], A Hadi Syafrudin[3], Agus Herawan[4], Rommy Hartono[5], Satriya Utama[6], Rakhmat Yatim[7], Rifki Ardinal[8], Bambang Sigit Pamadi[9]

[1]Satellite Technology Center, National Institute of Aeronautics and Space (LAPAN), Indonesia

e-mail: sartika.salaswati@lapan.go.id

Received: 21-08-2021. Accepted: 02-12-2022. Published: 27-12-2022

Abstract

Line Imager Space Application (LISA) is a multispectral camera on the LAPAN-A3/IPB satellite. This camera is the main payload that supports the remote sensing mission of the LAPAN-A3/IPB satellite. LISA has an important role in the payload system, that requires a good quality of camera. Vicarious calibration is one of several ways to get a good quality of camera. Vicarious calibration of LISA in the Jaddih hill area has been done without aerosol optical depth data. Therefore, further research was conducted to determine the effect of AOD data on the radiance coefficient. This paper describes the vicarious calibration of LISA using three types of data, namely LISA image, reflectance, and aerosol optical depth data of the Jaddih hill area. From the data types, the radiance coefficient for each LISA channel was obtained. The results show that there is an effect of AOD data on the radiance coefficient, but the negligible. The differences of the radiance coefficients are 5,634 %; 5,670 %; 9,774 % and 7,143 % for red channels, green channels, blue channels, and NIR channels respectively.

Keywords: *Aerosol Optical Depth (AOD), LAPAN-A3/IPB satellite, LISA image, multispectral camera, radiance coefficient, reflectance*

1. Introduction

Line Imager Space Application (LISA) is a multispectral camera on the LAPAN-A3/IPB satellite. This camera is the main payload that supports the remote sensing mission of the LAPAN-A3/IPB satellite. This camera has blue, green, red, and near-infrared (NIR) channels, with a ground resolution of 15 meters and 120 km swath-width from 510 km altitude. Besides, this camera has 16-bit radiometric resolution and 21 days of temporal resolution. In its application, LISA imagery has been used quite extensively, including to identify plant and plant growth types (Wijayanto et al., 2019), drought monitoring areas (Amalo et al., 2019), calculating the amount of chlorophyll plant (Permatasari et al., 2019), rice field monitoring (Raimadoya et al., 2011)(Setiawan et al., 2018), and land use analysis(Nugroho et al., 2019).

Since LISA imagery has been widely used, it requires high-quality geometric and radiometric image correction. To get this quality, it is necessary to perform a geometric and radiometric calibration process. Several calibration processes before launch have been carried out, including image focus calibration (Tahir et al., 2018), radiometric calibration modeling(S. Salaswati, 2016), and radiometric calibration in laboratories (Syafrudin et al., 2018). Image correction algorithms have been developed to make systematic corrections to satellite raw images (Hakim et al., 2019). Moreover, radiometric calibration has been carried out after the satellite was launched (vicarious calibration) to determine changes in the quality of cameras in orbit (Arai et al., 2019). Several studies related to vicarious radiometric calibration have been carried out in several homogeneous areas in Indonesia, including the Kupang cement mine area (Arai et al., 2019), Bromo Tengger Semeru National Park (Sartika Salaswati et al., 2019), and Jaddih Hill Madura (Sartika Salaswati et al., 2020). However, this study is still underway, with its shortcomings which there was no atmospheric data.

Aerosols are liquid or solid particles suspended in the atmosphere. Aerosols modify the energy budget of the earth-atmosphere system in several ways. They directly scatter

and absorb solar and thermal infrared radiation (Bohren, 1983)(Coakley, 1983)(Charlson, 1992), modify amount, lifetime, and microphysical and radiative properties of clouds and therefore indirectly change the Earth-leaving radiation (Twomey, 1977)(Albrecht, 1989)(Lensky & Rosenfeld, 2003). Aerosol Optical Depth (AOD) is a measure of extinction of radiation by aerosols due to absorption and scattering. It depends on the chemical composition and size of aerosol particles, and thus varies with the wavelengths of radiation. It also depends on the amount of aerosol in the atmosphere, and as such it is also a measure of aerosol loading (Laszlo & Liun, 2019).

Because of the influence of AOD on Earth-leaving radiation, AOD data should be used to support the vicarious radiometric calibration to minimize its effect. AOD is the basic parameter of radiative transmission and atmospheric correction, and affects the accuracy of radiometric calibration and atmospheric correction of satellite remote sensors (Huang, D.; Li, X.; Zhang, Y.; Zhang, 2019). This paper describes the effect of AOD data on the vicarious radiometric calibration of LISA LAPAN-A3. In this study, we generate radiance coefficients with AOD data then compared them with radiance coefficient without AOD data. The next purpose of this study is to improve the image quality of LISA LAPAN-A3 so that it can be used more widely.

2. Method

2.1. Time and Location

Two types of data measurements required for vicarious calibration were carried out on 30 October 2018 at 01:59:30 - 02:00:33 UTC. This time coincided with the passage of the LAPAN-A3 satellite at the specified location, namely the Jaddih Hill Madura (located at 7°5'0.04 and 112°45'38.49). The area was chosen because it met the requirements to be used as a calibration area. These requirements include good homogeneity (the Jaddih hill area is dominated by a homogeneous stretch of lime sand), has a high reflectance value (Jaddih hill is a limestone hill that is dominated by bright color, since the brighter objects, the higher reflectance). The next requirement is an area that is sufficient for the sensor resolution scale to be calibrated (has more than 30 m x 30 m based on Google Earth). Moreover, it has low rainfall. Based on images obtained by LISA in August - October 2018, hill area Jaddih Madura tends to be cloud-free. Finally, it can be accessed easily, since the Jaddih hill area is a tourist spot that can be accessed easily without complicated bureaucracies (Sartika Salaswati et al., 2020).

2.2. Instrumentation

The instrumentation or measuring instruments used in this study were a spectrometer and a sunphotometer. The spectrometer is used to measure ground reflectance while the sunphotometer is used to measure atmospheric components in the vicarious calibration region (Jaddih Hill Madura). The type of spectrometer is ASD's FieldSpecHand Held 2 type.

Meanwhile, the type of sunphotometer used is Microtops II from Solar Light Co. Ltd. This instrument is a handheld instrument with 5 channels to measure aerosol optical depth (AOD) more easily, accurately, and reliably. This multispectral instrument is designed to measure direct solar irradiance in 5 selected wavelength channels. These measurements provide information on atmospheric properties such as AOD and water vapor. Standard wavelengths are available from 340 nm, 380 nm, 440 nm, 500 nm, 675 nm, 870 nm, 936 nm, and 1020 nm. In this study, 440 nm, 500 nm, 675 nm, 870 nm, and 936 nm wavelengths were used. The wavelength was chosen because this study focuses on measuring atmospheric properties, especially the AOD and water vapor. The instruments and specifications are shown in Figure 2.1, Table 2.1, and Table 2.2.

(a) (b)

Figure 2.1. (a) Spectrometer HH2 ASD, (b) Sunphotometer Microtops II

Table 2.1. Spectrometer HH 2 ASD Spesification (ASD, 2010)

Spesification	Value
Wavelength Range	325 – 1075 nm
Wavelength Accuracy	± 1 nm
Spectral Resolution	< 3 nm at 700 nm
Integration Time	8.5 ms minimum (selectable)
Field-of-View	25^0 (Optional fore optics available)
Sampling Interval	1.5 nm for the spectral region 325 – 1075 nm
Spectrum File Size	Approximately 30 KB
Memory Storage	Up to 2000 spectrum files
Wigth	1.2 kg (2.6 lbs) with batteries
Body Dimensions	Measurements with handle not attached (width x depth x height) : 90 x 140 x 215 mm (3.5 x 5.5 x 8.5 in)
Temperature Range	Operating Temperature : 0^o to 40^o C (32^o to 104^o F) Storage Temperature : 0^o to 45^o C (32^o to 113^o F) Operating and Storage Humidity : 90 % Noncondensing

Table 2.2. Sunphotometer Microtops II Spesification (Solar Light Company, 2011)

Spesification	Value
Resolution	0,01 W/cm^2 on 305 nm Channel
Dynamic Range	>300,000
Viewing Angle	2.5^o
Precision	1-2%
Non-linearity	Max 0.002% FS
Operating Environment	0 to 50^{o}C, No Precipitation
Computer Interface	RS232 / USB with Adapter
Power Source	4xAA Alkaline Batteries
Weight	21 oz. (600 grams)
Size	4”W x 8”H x 1.7”D (10x20x4.3 cm)

2.3. Reflectance and Atmospheric Measurements

Reflectance measurements were carried out using a spectrometer with a pattern as shown in Figure 2.3

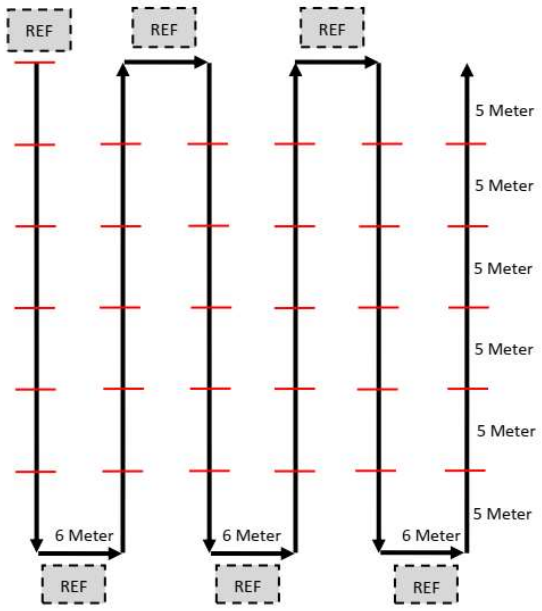

Figure 2.2. Reflectance Measurement Setup (Sartika Salaswati et al., 2020)

The word "REF" in Figure 2.3 shows that the reference data was taken at calibration site, that is Spectralon reflectance data. Meanwhile, the red line shows the location of the reflectance data sampling. Measurements with this pattern are expected to represent the reflectance value of a homogeneous area.

Measurements of atmospheric properties were carried out simultaneously with reflectance measurements at the same location. Measurement samples were taken several times with time variations by centering the sunphotometer with the sun's light point. The thing that needs to be considered in image acquisition, reflectance measurements, and atmospheric property measurements for this calibration are sky conditions. The sky must be cloudless to produce accurate data. Measurements of reflectance and atmospheric properties in the Jaddih Hill Madura can be seen in Figure 2.3.

Figure 2.3. Reflectance and Atmospheric Property Measurements at Jaddih Hill Madura

2.4. Data Processing

Data processing was carried out to produce the radiance coefficient. However, there are several stages of processing and calculations to provide the radiance coefficient.

2.4.1. TOA Radiance

TOA radiance is the first parameter that must be known to produce the radiance coefficient from satellite images. To produce this parameter requires reflectance data and aerosol optical depth (AOD). The reflectance data were obtained from spectrometer measurements that were averaged for each measurement. While the AOD was obtained from the 2-1 equation.

$$\tau_A = \frac{-LnV+LnV_0-m\,(\tau_R+\tau_{O_3})}{m} \quad (2\text{-}1)$$

τ_A is AOD, V is the signal received by the sunphotometer, V_0 is the extraterrestrial radiance, m is the air mass, τ_R and τ_{O_3} are Rayleigh and Ozone optical depth. Rayleigh OD is generated from calculations based on atmospheric pressure measurement data, water OD is obtained from MODTRAN (by selecting a typical tropical atmosphere model)(Arai et al., 2019), Ozone OD is obtained from a predetermined website (Arai et al., 2019), while the total OD is obtained from the summation Aerosol, Ozone, and Rayleigh optical depth. To do this calculation, a Langley's graph is required. Langley's graph is a representation of the sunphotometer calibration where the normal logarithm function of signal (Ln V) is proportional to the air mass (AM) (2-1 equation).

Reflectance and AOD become the MODTRAN software input to produce TOA irradiance. TOA irradiance is converted into TOA radiance using camera parameters (S. Salaswati, 2016). After obtaining the TOA radiance, we can know the TOA radiance for each channel based on the channel spectral (Arai et al., 2019). TOA radiance processing can be seen in Figure 2-4.

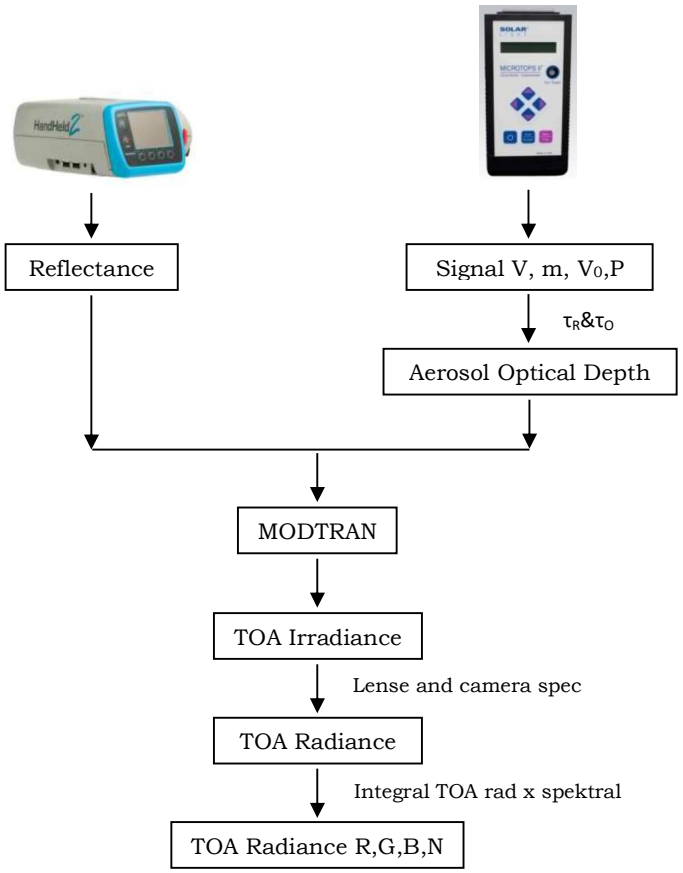

Figure 2.4. TOA Radiance Processing for Vicarious Radiometric Calibration

2.4.2. Radiance Coefficient

Following image acquisitions and TOA radiance processing, the radiance coefficient can be generated. The radiance coefficient calculation based on the following equation :

$$K_A = \frac{L - K_B}{DN} \quad (2\text{-}2)$$

K_A is radiance coefficient, DN is digital number of image, K_B is dark image data, and L is TOA radiance. If $K_B = 0$, the radiance coefficient on the LISA LAPAN-A3 is:

$$K_{AR} = \frac{L_R}{DN_R} \quad (2\text{-}3)$$

$$K_{AG} = \frac{L_G}{DN_G} \quad (2\text{-}4)$$

$$K_{AB} = \frac{L_B}{DN_B} \quad (2\text{-}5)$$

$$K_{AN} = \frac{L_N}{DN_N} \quad (2\text{-}6)$$

K_{AR}, K_{AG}, K_{AB}, and $K_{AN}$is radiance coefficient for each channel (red, green, blue, NIR). DN_R, DN_G, DN_B, DN_Ni s digital number of LISA image for each channel (red, green, blue, NIR). L_R, L_G, L_B, dan L_N is TOA radiance for each channel (red, green, blue, NIR).

3. Result and Discussion

3.1. Image of LISA LAPAN-A3, Jaddih Hill Madura

The LISA LAPAN-A3 image acquisition was carried out on 29-31 October 2018, but the image on 29 October 2018 cannot be used because there are thick clouds in the pixels of the calibration area. The image and calibration site are shown in Figure 3.1 and Figure 3.2.

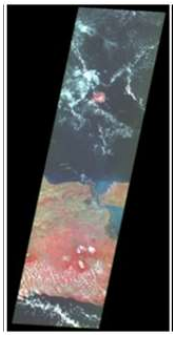

Figure 3.1. Image of LISA LAPAN-A3, Jaddih Hill Madura (30 October 2018)

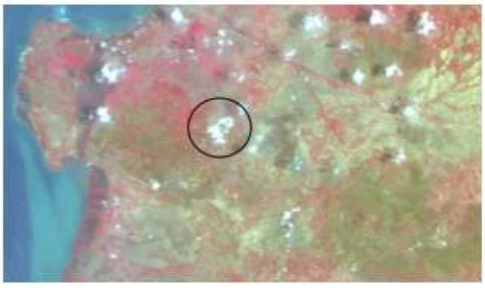

Figure 3.2. Calibration Site, Jaddih Hill Madura on LISA LAPAN-A3 Image (30 October 2018)

In Figure 3.2, it can be seen that the calibration area is dominated by almost white colors and uniform. The measurement area at the calibration site is 30 m x 30 m, it represents a 2 x 2 pixels calibration site image. From the data processing, the digital number (DN) for each channel is obtained as follows:

Table 3.1. Digital Number (DN) of LISA LAPAN-A3 Image on Calibration Site

Pixel	Red	Green	Blue	NIR
1	45477	33683	11238	23526
2	42883	34102	11392	22903
3	45436	34541	11452	23867
4	43301	35018	11643	23159
Average	**44274**	**34336**	**11431**	**23363**

3.2. Aerosol Optical Depth (AOD)

From atmospheric measurement using a sunphotometer, some measurement data was obtained. Measurement data were obtained are the coordinates, pressure, angle of collection data, air mass, sunphotometer signal (mV), and water vapor content at the measurement location. The data is processed to produce a Langley graph (Figure 3.3) and an Optical Depth graph (Figure 3.4) obtained from the calculation results.

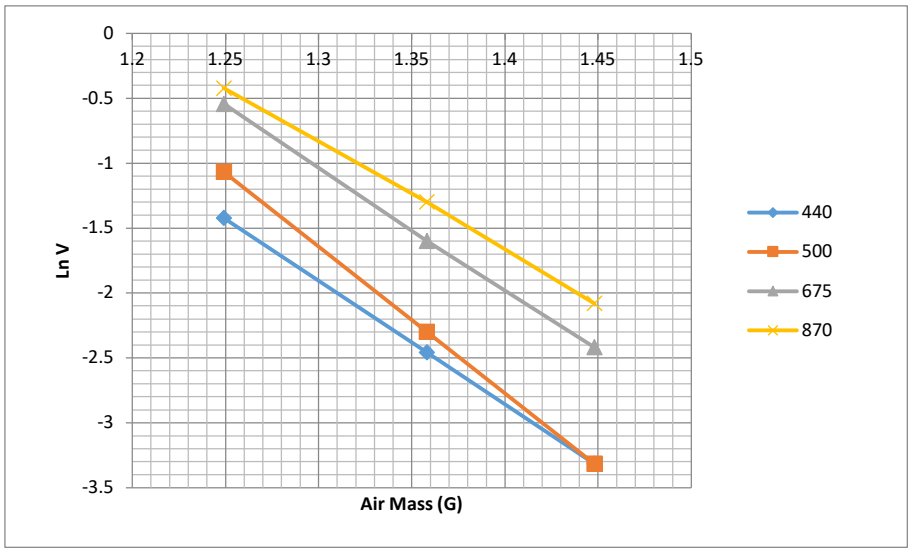

Figure 3.3. Langley Graph from Atmospheric Measurement for Wavelength 440 nm, 500 nm, 675 nm, and 870 nm (Jaddih Hill Madura, 30 Oct 2018)

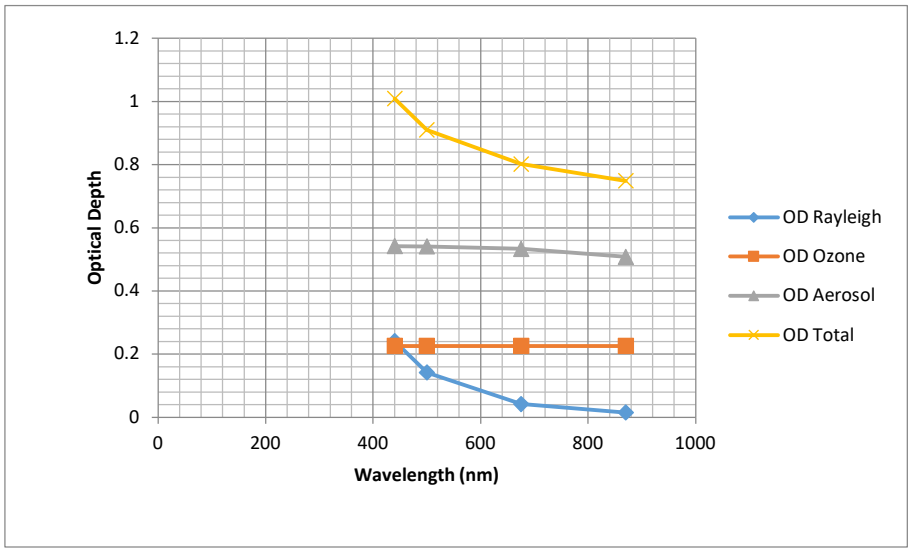

Figure 3.4. Optical Depth Graph Based on Calculation Result. ODR (Optical Depth Rayleigh), ODO (Optical Depth Ozone), ODA (Optical Depth Aerosol), and ODT(Optical Depth Total)

Figure 3.3 shows the Langley graph from atmospheric measurement using the sunphotometer. It can be seen, that the greater the air mass, the smallerthe natural logarithm signal derived from the sunphotometer. Meanwhile, a higher wavelength produces a natural logarithm with a larger value. However, the graph is not too precise because it only has three good data samples. This is because the atmospheric data obtained from measurements tend to be random so that from some samples only three data measurements can be used. Figure 3.4 shows an optical depth graph to the wavelength. From the graph, the highest optical depth is the total optical depth which is the sum of aerosol, ozone, Rayleigh optical depths. The second order is aerosol optical depth, which is the dominant optical depth compared to Rayleigh and Ozone optical depth. It is the input of the TOA radiance calculation process. Meanwhile, the next sequence is occupied by the Ozone and Rayleigh optical depth, which are other components contained in the total optical depth. From the graph, it can be seen, that the higher wavelength, the lower optical depth.

3.3. TOA Radiance

TOA radiance was obtained from data processing using MODTRAN software. This process requires input data, namely measurement conditions, reflectance data, and aerosol optical depth data obtained from previous calculations. From this process, TOA irradiance was generated with AOD variations for each channel. After that, TOA irradiance was converted into TOA radiance using lens and camera specifications (S. Salaswati, 2016). To find out the TOA radiance for each channel, it can be calculated with the integration of TOA radiance multiplied by each LISA spectral response (Arai et al., 2019). The TOA irradiance and TOA radiance graphs are shown in Figures 3.5 and 3.6. Meanwhile, the TOA radiance value of the LISA LAPAN-A3 for each channel is shown in table 3.2.

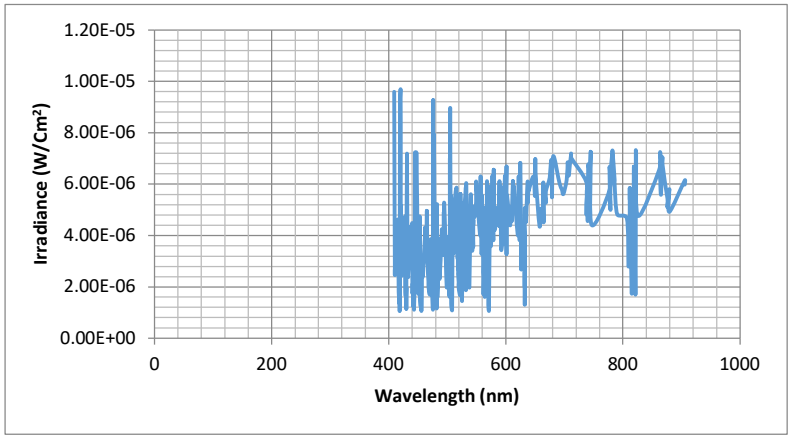

Figure 3.5. TOA Irradiance Graph for Vicarious Calibration of LISA LAPAN-A3

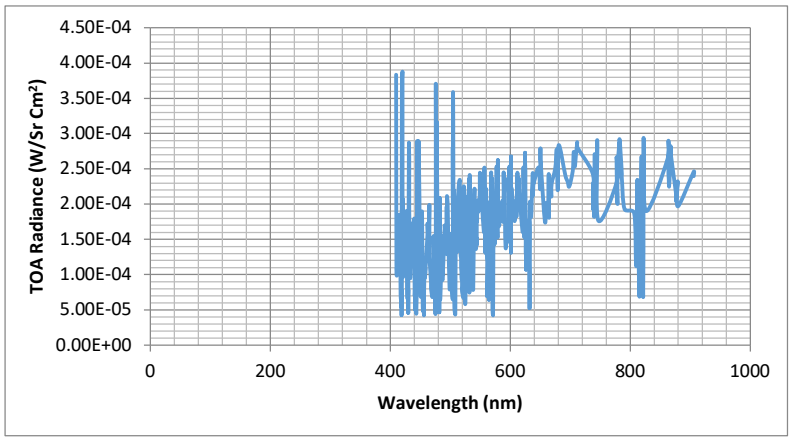

Figure 3.6. TOA Radiance Graph for Vicarious Calibration of LISA LAPAN-A3

Table 3.2.LISA Radiance Comparison of LAPAN-A3 Satellite on Jaddih Hill Madura Imagery (with and without AOD Data (Sartika Salaswati et al., 2020))

Channel	TOA Radiance (with AOD)	Radiance (without AOD)	Difference (%)
	mW/ Cm²-Sr-µm		
Red	62,750	59,229	5,611
Green	66,512	62,690	5,746
Blue	45,678	41,155	9,902
NIR	35,918	33,404	6,999

Table 3.3. LISA Radiance Comparison of LAPAN-A3 Satellites at the Jaddih Hill, Kupang (Arai et al., 2019), and Laboratory (Syafrudin et al., 2018)

Channel	TOA Rad Jaddih	TOA Rad Kupang	Rad Lab
	mW/ Cm²-Sr-µm		
Red	62,750	83,500	89,885
Green	66,512	87,550	92,452
Blue	45,678	50,640	52,472
NIR	35,918	37,000	40,909

The TOA radiance (with AOD) shows the top of atmosphere (TOA) radiance of the Jaddih hill region using a spectrometer and sunphotometer data, while the radiance (without AOD) shows the radiance of the Jaddih hill region using spectrometer data only. It can be seen in the table that the TOA radiance (with AOD) is greater than the radiance (without AOD). Where in TOA radiance data (with AOD), sunphotometer data have been used to correct some of the existing atmospheric factors. And as the name implies, the TOA radiance is the radiance that is received by the satellite camera in orbit, it is different from radiance in previous studies (Sartika Salaswati et al., 2020) which is the radiance received by the spectrometer instrument from ground measurements. Besides, we can also see in the table that the smallest difference is in the NIR channel which is the best channel on the LISA LAPAN-A3, then followed by the red, green, and blue channels.

Table 3.2 shows the radiance comparison of the Jaddih hill Madura area. Table 3.3 shows that the TOA radiance from this study is smaller than TOA radiance with the Kupang area calibration site and the radiance (in the laboratory). This is caused by, the Kupang area is more homogeneous than the Jaddih hill area. The Kupang calibration site is a flat cement surface while the Jaddih hill is a limestone area that less flat. Besides, based on ground measurements with a spectrometer, the Kupang cement mining area has a higher reflectance value than the Jaddih hill reflectance. Meanwhile, when it is compared in laboratory calibration, the radiance in the laboratory is greater than this study because the laboratory using the ideal light source. Besides, laboratory calibration has no interference during launch or when in outer space. So that the possibility of radiometric distortion is less.

3.4. Radiance Coefficient

After the TOA radiance is generated from the previous data processing. Furthermore, data processing is carried out to produce the LISA radiance coefficient. The radiance coefficient is a coefficient to convert the digital number (DN) of the image in radiance units. This radiance value is then widely used in remote sensing applications. The radiance coefficients in this study and comparisons with previous studies are shown in Tables 3.4 and 3.5.

Table 3.4. Radiance Coefficient Comparison (With and Without Aerosol Optical Depth)

Channel	Rad Coefficient (With AOD)	Rad Coefficient (Without AOD)	Difference (%)
Red	0,00142	0,00134	5,634
Green	0,00194	0,00183	5,670
Blue	0,00399	0,00360	9,774
NIR	0,00154	0,00143	7,143

Table 3.5. Radiance Coefficient Comparison LISA LAPAN-A3 at the Jaddih Hill, Kupang (Arai et al., 2019), and Laboratory (Syafrudin et al., 2018)

Channel	Radiance Coefficient		
	Jaddih Hill Madura	Cement Mine Kupang	Laboratory
Red	0,00142	0,00312	0,00074
Green	0,00194	0,00569	0,00060
Blue	0,00399	0,01191	0,00151
NIR	0,00154	0,00486	0,00085

Table 3.6. The Difference in The Radiance Coefficient of LISA LAPAN-A3

Channel	The Difference in The Radiance Coefficient (%)	
	| Jaddih Hill – Cement Kupang |	|Jaddih Hill - Laboratory |
Red	54,487	47,887
Green	65,905	69,072
Blue	66,498	62,155
NIR	68,312	44,805

Table 3.4 shows the radiance coefficient with and without using AOD data. From the table, it can be seen that coefficients are produced with and without AOD data are not much different. This can be seen that the difference value tends to be small. Thus, it is seen that there is an effect of AOD data on the radiance coefficient, but the effect is negligible. This is consistent with other satellite calibrations which state that the vicarious calibration uncertainty for FY-3D/MERSI-II is only affected by AOD as much as 2% (Chen et al., 2021).

While table 3.5 shows the radiance coefficient comparison with previous research and table 3.6 shows the difference in the radiance coefficient. Table 3.5 shows that the blue channel has the biggest radiance coefficient compared to other channels. This is because the DN value generated by the blue channel is smaller than the other channels. In LISA LAPAN-A3 the blue channel is less sensitive to detecting objects than other channels. In the table, it can be seen that the LISA radiance coefficient produced in this study is approximately 2 - 3 times smaller than the radiance coefficient at the Kupang site and 2 - 3 times greater than laboratory measurements. In addition, table 3.6 shows a fairly large percentage difference. In other words, the coefficient of radiation generated in this study needs to be studied further.

4. CONCLUSION

Analysis of the atmospheric effect on the vicarious radiometric calibration of the LISA LAPAN-A3 was carried out. Based on the description that has been presented in the previous section, we confirm that there are differences in the radiance coefficient values are generated using AOD data and without using AOD data. However, the difference is negligible. The difference in the radiance coefficient on the red channel is 5,634 %; green channel 5,670 %; blue channel 9,774 %, and NIR channel 7,143 %. While the results of comparison with other studies show a fairly large percentage difference (table 3.6). Therefore, the results of this study still need to be studied further.

Acknowledgements

The author would like to thank Mr. Mujtahid as the head of LAPAN Satellite Technology Center, as well as Mr. Wahyudi Hasbi as chief engineer of the satellite operation missions, for their support and assistance so that this works can be well completed.

Contributorship Statement

Sartika Salaswati, Patria Rachman Hakim, and A Hadi Syafrudin have the same role as the main contributors in this research, who are responsible for the research design process and calibration procedures, as well as processing and analysis of the data. Meanwhile, Rommy Hartono, Satriya Utama, Agus Herawan, Rifki Ardinal, Rakhmat Yatim, and Bambang Sigit Pamadi acted as member contributors in this study, who are responsible for the data acquisition process and data measurements in the field.

References

Albrecht, B. A. (1989). Aerosols, cloud microphysics, and fractional cloudiness. *Science*, *245*(4923), 1227–1230. https://doi.org/10.1126/science.245.4923.1227

Amalo, L. F., Nur, I. A., & Rochimawati, N. R. (2019). Drought monitoring using LISAT (LAPAN-IPB Satellite) and Landsat 8 Satellite Imagery in Pakisjaya District, West Java. *IOP Conference Series: Earth and Environmental Science*, *284*(1). https://doi.org/10.1088/1755-1315/284/1/012008

Arai, K., Hasbi, W., Hadi Syafrudin, A., Hakim, P. R., Salaswati, S., Prasetyo, L. B., & Setiawan, Y. (2019). Method for uncertainty evaluation of vicarious calibration of spaceborne visible to near infrared radiometers. *International Journal of Advanced Computer Science and Applications*, *10*(1), 387–393. https://doi.org/10.14569/IJACSA.2019.0100151

Bohren, C. F. (1983). Absorption and scattering of light by small particles. *Absorption and Scattering of Light by Small Particles*. https://doi.org/10.1088/0031-9112/35/3/025

Charlson, R. (1992). Climate Forcing by Anthropogenic Aerosols. *Science*, *255*, 423–230.

Chen, S., Zheng, X., Li, X., Wei, W., Du, S., & Guo, F. (2021). Vicarious radiometric calibration of ocean color bands for fy-3d/mersi-ii at lake qinghai, china. *Sensors (Switzerland)*, *21*(1), 1–18. https://doi.org/10.3390/s21010139

Coakley, J. (1983). The effect of tropospheric aerosols on the Earth's radiation budget: a parameterization for climate models. *J.Atmos.Sci*, *40*, 116–138.

Hakim, P. R., Syafrudin, A. H., Salaswati, S., Utama, S., & Hasbi, W. (2019). *Development of Systematic Image Preprocessing of LAPAN-A3/IPB Multispectral Images*. *7*(10), 9–18. http://arxiv.org/abs/1901.09189

Huang, D.; Li, X.; Zhang, Y.; Zhang, Q. (2019). Novel high-precision full autocontrol multi-waveband sun photometer. *J. Appl. Opt*, *40*, 109–113.

Laszlo, I., & Liun, H. (2019). EPS Aerosol Optical Depth (AOD) Algorithm Theoretical Basis Document. *NOAA NESDIS CENTER for SATELLITE APPLICATIONS and RESEARCH*, 1–79.

Lensky, I. M., & Rosenfeld, D. (2003). Satellite-based insights into precipitation formation processes in continental and maritime convective clouds at nighttime. *Journal of Applied Meteorology*, *42*(9), 1227–1233. https://doi.org/10.1175/1520-0450(2003)042<1227:SIIPFP>2.0.CO;2

Nugroho, S. P., Handayani, L. D. W., Meidiza, R., & Munggaran, G. (2019). Landuse change analysis for hydrology response and planning management of Cibeet Sub-Watershed, West Java, Indonesia. *IOP Conference Series: Earth and Environmental Science*, *284*(1). https://doi.org/10.1088/1755-1315/284/1/012002

Permatasari, P. A., Muslimah, S., & Utomo, B. A. (2019). Comparison of LISAT and Landsat imagery for estimating chlorophyll-a (case study: Jatiluhur Reservoir). *IOP Conference Series: Earth and Environmental Science*, *284*(1). https://doi.org/10.1088/1755-1315/284/1/012041

Raimadoya, M. A., Trisasongko, B. H., & Zain, A. (2011). Analisis Misi Dan Rancangan Lapan-Ipb Satellite (Lisat) Untuk Pemantauan Kemandirian Pangan. *Jurnal Ilmu Pertanian Indonesia*, *16*(3), 173–178.

Salaswati, S. (2016). *Simulation of Radiometric Correction of CCD KLI 8023*. LAPAN Satellite Technology Center Scientific Book.

Salaswati, Sartika, Hakim, P. R., Syafrudin, A. H., Hartono, R., & Utama, S. (2020). Vicarious Radiometric Calibration of Lapan-A3 / IPB Satellite Multispectral Imager in Jaddih Hill Madura. *Journal of Aerospace Technology*, 31–42.

Salaswati, Sartika, Suryanti, D. I., & Utama, S. (2019). Taman Nasional Bromo Tengger Semeru (TNBTS) Observation for Vicarious Calibration of LAPAN-A3 Multispectral Camera. *Proc. SIPTEKGAN XXIII*, *1*, 224–230.

Setiawan, Y., Prasetyo, L. B., Pawitan, H., Liyantono, L., Syartinilia, S., Wijayanto, A. K., Permatasari, P. A., Syafrudin, A. H., & Hakim, P. R. (2018). Pemanfaatan Fusi Data Satelit Lapan-a3/Ipb Dan Landsat 8 Untuk Monitoring Lahan Sawah. *Jurnal*

Pengelolaan Sumberdaya Alam Dan Lingkungan (Journal of Natural Resources and Environmental Management), *8*(1), 67–76. https://doi.org/10.29244/jpsl.8.1.67-76

Syafrudin, A. H., Salaswati, S., & Hasbi, W. (2018). Pre-Flight Radiometric Model of Linear Imager on LAPAN-IPB Satellite. *IOP Conference Series: Earth and Environmental Science*, *149*(1). https://doi.org/10.1088/1755-1315/149/1/012068

Tahir, A. M., Hakim, P. R., & Syafruddin, A. H. (2018). Peningkatan Kualitas Fokus Citra Imager Multispektral Satelit Lapan-a3 (Image-Focusing Quality Improvement on Lapan-a3 Satellite Multispectral Imager). *Jurnal Teknologi Dirgantara*, *14*(1), 37. https://doi.org/10.30536/j.jtd.2016.v14.a2946

Twomey, S. (1977). The Influence of Pollution on The Shortwave Albedo of Clouds. *J. Atmos. Sci.*, *34*, 1149–1152.

Wijayanto, A. K., Yusuf, S. M., & Pambudi, W. A. (2019). The Characteristic of spectral reflectance of LAPAN-IPB (LAPAN-A3) Satellite and Landsat 8 over agricultural area in Probolinggo, East Java. *IOP Conference Series: Earth and Environmental Science*, *284*(1). https://doi.org/10.1088/1755-1315/284/1/012004